The muscarinic acetylcholine receptor in dermal papilla cells regulates hair growth

Gary K.W. Yuen[1,2], Kevin Q.Y. Wu[1,2], K.W. Leung[1,2], Queenie W.S. Lai[1,2], Sybil Y.J. Xia[1,2], Maggie S.S. Guo[1,2], Alex X. Gao[1,2], Janet Y.M. Ho[1,2], Harry C.T. Chu[1,2], Karl W.K. Tsim[1,2*]

[1]Division of Life Science, Centre for Chinese Medicine, and State Key Laboratory of Molecular Neuroscience, The Hong Kong University of Science and Technology, Hong Kong, China

[2]Shenzhen Key Laboratory of Edible and Medicinal Bioresources, HKUST Shenzhen Research Institute, Shenzhen 518057, China

[*]Correspondence author

Prof. Karl Tsim, Division of Life Science and Center for Chinese Medicine, The Hong Kong University of Science and Technology, Clearwater Bay, Kowloon, Hong Kong, China

Tel: +852 2358 7332;

Fax: +852 2358 1559;

Email: botsim@ust.hk

Abstract

The role of cholinergic system in hair biology is poorly understood. In M4 muscarinic receptor (mAChR) knockout mice, the hair follicles have a prolonged telogen phase and failed to produce hair shafts. Here, we reported that hair growth was regulated by cholinergic system via mAChRs. Dermal papilla cells expressed different cholinergic biomarkers. Inhibiting AChE or stimulating mAChR in dermal papilla cells, culture vibrissae and skin epidermis promoted the hair growth. In cultured papilla cells treated with bethanechol, an agonist of mAChR, an activation of Wnt/β-catenin signalling was illustrated by various indicative biomarkers, including phosphorylation of GSK-3β and mRNA expression of various molecules for Wnt/β-catenin signalling. Activation of Wnt/β-catenin signalling was mediated by PI3K/AKT and ERK signalling upon the stimulation of bethanechol. In addition, an increase in hair shaft elongation was observed in mouse vibrissae upon the treatment of bethanechol, suggesting the cholinergic role in hair growth.

Introduction

In non-neuronal cells, the cholinergic system, composing acetylcholine (ACh) synthesizing enzymes, transporters, receptors, and degrading enzymes, exhibits a wide range of biological roles on different organs and pathologies(Beckmann & Lips, 2013; Grando, 2007; Kurzen et al., 2007; Wessler & Kirkpatrick, 2008). Several lines of evidence suggest the dysregulation of cholinergic system in different tissues is leading to diverse diseases, having significant implications for human health. For an example in skin epidermis, the role of cholinergic molecules has been proposed to be involved in different skin functions(Grando et al., 1993; Guo et al., 2023). A synapse-like interplay between melanocyte and keratinocyte, named as “skin synapse”, has been proposed(Wu, Bai, et al., 2020; Wu et al., 2018; Wu, Xia, et al., 2020). The direct involvement of cholinergic molecules is directing skin melanogenesis in both melanocyte and keratinocyte. Under the exposure to UV, keratinocyte is stimulated to release ACh acting on acetylcholine receptor (AChR) localized on melanocyte to trigger the synthesis and release of melanin. In parallel, patients suffering from atopic dermatitis showed over 14 folds higher level of ACh in epidermis and dermis, as compared to normal levels(Heyer et al., 1997; Wessler et al., 2003).

In mammalian skin, hair follicle is an organ found in skin dermal layer. The hair follicle, containing over 20 different cell types, is responsible for hair growth via a complex and dynamic process(Bernard, 2006). The hair growth is tightly regulated by the follicle in a cyclic manner(Lin et al., 2022), which consists of three distinct phases, namely: (i) anagen (the active hair growth phase); (ii) catagen (the regression phase); and (iii) telogen (the resting phase), which are characterized by unique morphological and molecular features(Oh et al., 2016; Paus & Cotsarelis, 1999). To achieve a well-balance between hair growth and regression, a range of growth inhibiting and/or

promoting signals are involved in regulating different phases of hair follicle. Among those growth promoting signals, wingless (Wnt), fibroblast growth factor (FGF), vascular endothelial growth factor (VEGF), and insulin-like growth factor 1 (IGF-1), have been identified as key players in promoting hair growth(Lin et al., 2015; Natarelli et al., 2023; Yano et al., 2001). In contrast, the inhibiting signals, such as transforming growth factor β (TGF-β) and bone morphogenetic protein (BMP), are known to drive hair follicle into regression(Hibino & Nishiyama, 2004; Rendl et al., 2008; Sharov et al., 2005). Activation of Wnt/β-catenin signaling triggers the growth of hair follicles by stimulating different gene expressions at the anagen phase(Andl et al., 2002; Beaudoin III et al., 2005; Huelsken et al., 2001; Kishimoto et al., 2000). The dermal papilla cell (DPC), a group of specialized mesenchymal cells clustering at the base of hair follicle, is a crucial player in regulating hair growth(Yang & Cotsarelis, 2010): this cell secretes a range of paracrine and autocrine factors, including Wnt, R-spondin, FGF, and Noggin, acting on the follicular bulge stem cells to initiate the anagen phase, as well as to promote hair growth(Driskell et al., 2011; Matsuzaki & Yoshizato, 1998; Morgan, 2014).

The role of the cholinergic system in hair biology remains an interesting topic with limited research, having only a few reports exploring the relationship of the complex process. Several lines of evidence support the notion of ACh playing role in hair biology. Alzheimer's patients taking oral reversible and competitive acetylcholinesterase (AChE) and butyrylcholinesterase (BChE) inhibitor, rivastigmine, exhibited symptoms of hypertrichosis and hair re-pigmentation(Chan et al., 2020; Imbernón-Moya et al., 2016; Müller, 2007). In DPCs treated with AChE inhibitor, nor-galantamine, a stimulation of anagen's activating signalling has been identified(Kowal et al., 2018; Prvulovic et al., 2010; Scott & Goa, 2000; Yoon et al., 2019). In addition,

the knockout mice of M4 muscarinic receptor (M4 mAChR) showed a defect in hair growth: the hair follicles had a significantly prolonged telogen phase, and which failed to produce pigmented hair shafts(Hasse et al., 2007; Takahashi, 2021). These findings provide supporting evidence that the cholinergic system may play roles in the multifaceted processes of hair growth. Having these lines of evidence, we propose a hypothesis that the cholinergic signalling in hair follicles is able to regulate hair growth. Here, the expression profiles of cholinergic molecules in DPCs and hair follicle were determined. In addition, the release of ACh, induced by solar light, from DPC was demonstrated, which thereafter activated the AChRs localized on DPCs. The cholinergic activation triggers the Wnt/β-catenin signalling to promote hair growth. These findings shed light on the role of cholinergic system in hair growth.

Results

1. Characterization of cholinergic molecules in DPC

DPC was employed here as the major cell type in testing the induction of hair growth. The cultures showed a rapid growth from day 2 to 6 after plating: the maximal cell number was at day 7 (**Supplementary Fig. 1A**). The cultures of DPC contained mainly the enzymatic activity of AChE instead of BChE, as revealed by the effect of different specific inhibitors (**Supplementary Fig. 1B**). The expressions of cholinergic molecules in cultured DPCs were identified, and these molecules showed changes during the growth. Specifically, AChE activity was decreased, while BChE activity was increased as the culture time progressed (**Fig. 1A**). This pattern was in line with expressions of protein and mRNA of AChE and BChE, indicating a potential regulatory mechanism governing the expressions of these two enzymes (**Fig. 1B&E**). The mRNA expression of choline acetyltransferase (ChAT) was unchanged during the growth

period (**Fig. 1C**). The mRNA expressions of M4 mAChR and alkaline phosphatase (ALP) were decreased in the first 48 hours of culture and increased thereafter.

The molecular form of AChE in the cultures was determined by a sucrose density gradient, and the results revealed the presence of amphiphilic monomer (G_1), dimer (G_2) and tetramer (G_4) (**Fig. 1D**). Notably, the G_4 AChE was found to be the major form. The mRNA expression of BChE was higher than that of AChE by over 30% (**Fig. 1F**). The enzymatic activity of AChE was ~ 6 times higher than that of BChE (**Fig. 1G**). The hydrolysing rate of ACh was much faster by AChE than that of BChE, and therefore, AChE should still play a dominant role in breaking down ACh here. The mRNA expressions of AChE, BChE and ChAT in different cell lines were compared by qPCR. AChE mRNA expression of DPC was much lower than that of HaCaT and SH-SY5Y cells (**Supplementary Fig. 1C**). In addition, the identification of subunits for nAChR and mAChR, as well as other cholinergic molecules in DPC, was done by specific primers in PCR. **Supplementary Fig. 2A-C** shows the presence of these molecules.

2. DPC as a source of ACh

ChAT is an enzyme known for its pivotal role in the synthesis of ACh. While vesicular ACh transporter (VAChT) is a crucial neurotransmitter transporter responsible for sequestration of ACh into secretory organelles, i.e., synaptic vesicle, in neurons. To confirm the presence of cholinergic molecules in DPC, immunofluorescent staining was performed. In the present of Triton X-100, the expressions of ChAT, VAChT and SYP in DPCs were recognized by using anti-ChAT, anti-SYP and anti-VAChT antibodies (**Fig. 2A**). The staining of SYP was localized intracellularly in a punctate manner.

Dermal papilla is the regulating centre in hair follicle, which secretes growth factors to stimulate the development of hair follicle. Here, we hypothesized that DPC could be the source of ACh in activating cholinergic system in hair follicle. To support this hypothesis, the light sensitive protein should be present in the DPC. Opsin has been proposed in sensing light by skin surface, as to cause ACh release from epidermal cells (Wu, Xia, et al., 2020). The mRNAs encoding OPN1, OPN2 and OPN3 were identified in DPC; while the expressions of other opsins were not observed (**Fig. 2B**). The expression profile of these opsin was peaked at 1 day after culture (**Fig. 2C**). To reveal the possible release of ACh from DPC, KCl was employed to depolarize the cell membrane. Starting from the concentration of 25 mM KCl, an increase of ACh in conditioned medium, released by DPC, was detected by an increase of ~2 folds (**Fig. 2D**). The treatment with KCl in DPCs resulted in the release of ACh over time, reaching a maximum at 15 min of the challenge (**Fig. 2E**). In addition, the exposure of solar light to DPCs was able to cause the release of ACh, and which was in a time-dependent manner, having a maximum at 5 min of the exposure (**Fig. 2F**). EDTA, a Ca^{2+} chelator, was able to block the light-mediated release of ACh, suggesting the involvement of Ca^{2+} in ACh release. In line to this notion, the amount of ACh in P7 anagen skin tissue was ~5 times higher than that of the P23 telogen skin tissue (**Fig. 2G**). Thus, the level of ACh in mouse skin was varied during the hair cycle. Besides, the pTOPflash plasmid containing TCF-binding sequence for β-catenin TCF complex was used to quantify the activation of Wnt/β-catenin, a key signal during hair growth. The exposure of solar light in pTOPflash-transfected DPC was able to increase the luciferase activity (**Fig. 2H**).

3. Cholinergic signalling in hair growth

The immunostaining analysis of cryosection of mouse skin showed the localizations of AChE and BChE in dermal papilla, indicated by SOX2 staining, at

anagen phase of hair growth cycle, which were however disappeared in telogen phase (**Fig. 3A,B**). Thus, AChE and BChE might function robustly during the anagen phase. Because of high expressions of the enzymes, the dermal papilla could be the centre of cholinergic signalling in hair follicle. As expected, AChE and BChE were recognized and localized on the DPC membrane (**Fig. 3C**). To support the role of cholinergic signalling in hair growth, the downstream targets of Wnt signalling, i.e., axin-related protein, (AXIN2), β-catenin, insulin-like growth factor-1 (IGF-1) and ALP, were measured in the present of BW284c51, an AChE inhibitor, for 48 hours in cultured DPCs (**Fig. 4A**). The mRNA levels of AXIN-2, IGF-1 and ALP were increased significantly in dose-dependent manners after the treatment of BW284c51. Moreover, the growth biomarker of DPC, the mRNA encoding ALP, was increased significantly by a maximum of ~2.5 folds. The mRNA level of IGF-1, a hair growth promoting factor, was increased by over 3 folds upon BW284c51 treatment. The recombinant Wnt3a served as a positive control here, as an agonist in activating the downstream genes of Wnt (**Fig. 4A**). On the other hand, the role of Wnt/β-catenin signalling in regulating the cholinergic molecules was determined. Valproic acid (VPA), an inhibitor of GSK-3β, activates Wnt/β-catenin signalling in cultured DPC. The mRNA expression of AChE was decreased by ~80% under the treatment of VPA, and BChE mRNA was increased by ~3 folds (**Fig. 4B**). The mRNA expression of ChAT was relatively unchanged. Bt_2-cAMP was served as a control in regulating AChE, BChE and ChAT expressions.

To determine the role of AChE inhibitor in hair growth, mouse vibrissae *ex vivo* cultures were used. The isolated vibrissae were treated with different concentrations of BW284c51 for 72 hours. As compared to the control, the length of hair, generated from the follicle being treated with BW284c51, was increased significantly in a dose-

dependent manner (**Fig. 4C**). The isolated vibrissae treated with 100 mM BW284c51 showed an increase of hair length by ~60%, as compared to the control. VPA served as a positive control showing an induction of hair length by ~45%, less than that of the AChE inhibitor (**Fig. 4C**).

4. The topical effect of cholinergic drugs in hair growth

To test the cholinergic system being involved in hair growth, the dorsal back of shaved mice was applied every day with the vehicle (negative control), 0.2 mM BW284c51, 25 mM bethanechol (an agonist of all subtypes of muscarinic receptors) and 5 mM VPA (a positive control). Here, the treatments of BW284c51, bethanechol and VPA exhibited an accelerated re-entry of anagen, as determined by hair growth in surface view and H&E cross-section (**Fig. 5A&B**). By histologic analysis, the dermis thickness and the hair weight, and the number of hair follicles were significantly increased under the treatments of BW284c51, bethanechol and VPA (**Fig. 5C-E**). By immunostaining analysis, the expression level of Ki67, a marker of cell proliferation in DPC, was significantly increased, at least by over 150%, in the hair matrix of follicle treated with BW284c51, bethanechol or VPA (**Fig. 5F&G**).

M4 muscarinic acetylcholine receptor (M4 mAChR) was expressed in hair follicle and DPC, as recognized by immunohistochemical staining (**Fig. 6A**). M4 mAChR was co-localized with SOX2, a marker of dermal papilla, indicated that M4 mAChR was expressed predominantly at the dermal papilla. Bethanechol was applied in cultured DCPs. The mRNA levels of Wnt signalling downstream genes, i.e., AXIN2, β-catenin, LEF-1, IGF-1, and ALP, were revealed by RT-PCR after the treatment. The results indicated that the levels of mRNAs encoding AXIN2, LEF-1, and β-catenin were significantly increased in a dose-dependent manner upon treatment with bethanechol (**Fig. 6B**). In parallel, the growth markers of DPC, e.g., IGF-1 and ALP, were increased.

In addition, bethanechol was applied in pTOPflash-transfected DPC, the luciferase activity was markedly induced in a dose-dependent manner after the treatment: the maximal induction was at ~5 mM bethanechol (**Fig. 6C**).

Pirenzepine (a M1 selective antagonist), gallamine (a M2 selective antagonist), 4-DAMP (a M3 selective antagonist), tropicamide (a M4 selective antagonist), and atropine (an antagonist of muscarinic receptors) were used here to identify the receptor specificity in responding to challenge of bethanechol. In pTOPflash-transfected DPC, the treatment with pirenzepine, gallamine, tropicamide did not induce luciferase activity. In DPC-treated with 4-DAMP, the luciferase activity was increased by ~40% (**Fig. 6D**). The pre-treatments with tropicamide and atropine were able to inhibit markedly the bethanechol-induced luciferase activity, suggesting the involvement of M4 mAChR. In line with the notion, the treatment of bethanechol in cultured hair follicles was able to induce hair growth in a dose-dependent manner: the maximal induction by over 80% was at 1 mM bethanechol (**Fig. 6E**). VPA served as a positive control.

GSK3β plays a crucial role in regulating Wnt signalling. GSK3 phosphorylates β-catenin, leading to its destabilization and subsequent degradation, thereby maintaining a low level of β-catenin in the cytosol and nucleus. Treating bethanechol in DPC was able to induce GSK3β phosphorylation at 5 min of incubation, while the pre-treatment of atropine or tropicamide was able to block the induction mediated by bethanechol (**Fig. 6F**). Besides, the GSK3β phosphorylation, induced by bethanechol, was in a transient manner (**Fig. 6G**). In contrast, VPA induced the phosphorylation at a rather substantial manner. Moreover, siRNA of M4 mAChR in DPCs was able to reduce the receptor expression by ~60% (**Fig. 6H**). In the siRNA transfected cultures, the levels of mRNAs encoding AXIN2, LEF-1, β-catenin and IGF-1, as induced by

applied bethanechol, were significantly decreased in a dose-dependent manner upon an increase dose of siRNA-M4 mAChR (**Fig. 6H**). The results suggested M4 mAChR could be a regulator of Wnt downstream signalling in DPC for hair growth.

5. Downstream signalling of M4 mAChR in hair growth

The M4 mAChR couples to $G_{i/o}$ protein leading to the inhibition of cAMP production by inhibiting adenylyl cyclase(Van der Westhuizen et al., 2021). By pre-treating pGloSensor-22F^{TM} plasmid, or pCRE-Luc, transfected DPC with forskolin, the increased luminescence, or luciferase, signal was inhibited by bethanechol in a dose-dependent manner (**Fig. 7A&C**). The pre-treatment with tropicamide was able to block the inhibition mediated by bethanechol, which further confirmed the involvement of M4 mAChR in DPC (**Fig. 7B&D**).

The interaction between M4 mAChR and Wnt signalling was poorly studied. We hypothesized that M4 mAChR alone can bypass the Frizzled and LRP5/6 receptors to activate the Wnt signalling. In pTOPflash-transfected DPC, the application of Wnt3a, or bethanechol, induced the promoter activity (**Fig. 8A**). Their activations were fully blocked by DKK-1 (an inhibitor of Wnt signalling binding to the LRP6 co-receptor), or tropicamide, respectively. The co-treatment of Wnt3a and bethanechol increased the luciferase activity by ~100%, higher than the single drug challenge. With the pre-treatment of DKK-1, or tropicamide, in pTOPflash-transfected DPC, the luciferase activity was inhibited partially in the co-treatment of Wnt3a together with bethanechol (**Fig. 8A**). Similar results were obtained in pTOPflash-transfected PC12, a neuronal cell line (**Supplementary Fig. 1E**). The co-treatment of Wnt3a and bethanechol induced the phosphorylation of GSK-3β by ~3 fold, higher than using the single drug. The pre-treatment of DKK-1, or tropicamide, inhibited partially the phosphorylation of GSK-3β triggered by the co-treatment (**Fig. 8B**), suggesting the two signalling events should

be independent. This result was further illustrated in *ex vivo* cultures of mouse vibrissae. Both Wnt3a and bethanechol stimulated hair growth. The co-treatment of Wnt3a and bethanechol increased the hair shaft length by ~80%. As expected, the pre-treatment of DKK-1, or tropicamide, partially inhibited the growth triggered by the co-treatment (**Fig. 8C**).

To investigate the relationship between mAChR and Wnt signalling pathways, different inhibitors, including H89 (PKA inhibitor), U73312 (PLCβ inhibitor), LY294002 (PI3K inhibitor), BIS (PKC inhibitor), U0126 (ERK/MEK inhibitor), were pre-treated to the cultured DPC, as to block the activation triggered by bethanechol. Treatments of LY294002 and U0126 were able to inhibit the effect of bethanechol, significantly (**Fig. 8D**). U73312 and BIS showed minor inhibition, but not at a significant level. The pathway of PI3K/AKT/mTOR are known to have a direct relationship with Wnt signalling via phosphorylation of GSK3β. Here, the treatment of bethanechol in DPCs induced the phosphorylation of AKT in a time-dependent manner and peaked at 5 min: this effect was fully inhibited by pre-treatment with LY294002 (**Fig. 8E&F**). Moreover, the bethanechol-induced GSK-3β phosphorylation was inhibited by the pre-treatment of LY294002 (**Fig. 8G**). This further verified the AKT could be the mediator between the signalling of M4 mAChR and Wnt pathway.

Discussion

For the first time, we have given a detailed mechanistic analysis of cholinergic system in regulating hair growth. Under the stimulation of solar light, ACh is being released from DPC, and which thereafter activates M4 mAChR, as well as Wnt signalling pathway, localized on DPC (**Fig. 9**). This stimulatory effect of Wnt signalling by M4 mAChR in promoting hair growth is mediated via PI3K/AKT and ERK/MEK

signalling pathways. Several lines of evidence support this notion: (i) the expression and localization of cholinergic molecules in DPC; (ii) induction of ACh release by solar light; (iii) activation of M4 mAChR triggering Wnt signalling and hair growth; (iv) blockage of hair growth by mAChR antagonist; and (v) regulation of cholinergic enzyme by Wnt agonist. Our findings support the relationship of hair pigmentation and hypertrichosis in the known therapy of having intake of cholinesterase inhibitors. For an example in Alzheimer's patients, 24 out of 62 patients reported hair darkening in the occipital region after using cholinesterase inhibitor for at least 6 months(Chan et al., 2020). In another example, a Caucasian 80-year-old male who received AChE/BChE inhibitor rivastigmine for one month was diagnosed acquired localized hypertrichosis on both forearms(Imbernón-Moya et al., 2016). These findings highlight the potential regulation of hair growth by cholinergic system. Having this hypothesis, the cholinergic molecules in hair follicles may be a potential therapeutic target for alopecia. Besides, AChE inhibitors are currently approved by the US Food and Drug Administration for the treatment of Alzheimer's disease, and in general these drugs are safe to use(McGleenon et al., 1999; Vecchio et al., 2021). To fully comprehend the potential of these inhibitors as an alopecia treatment, additional preclinical and clinical studies are required. Our studies raise the possibility that the cholinergic drug can be a new niche to cure alopecia.

Wnt signalling plays an important role in the growth and development of hair follicles. Here, we have demonstrated the activation of Wnt signal in DPC could be triggered by M4 mAChR. The relationship between cholinergic system and Wnt signalling has been reported in various cell types, but the detailed mechanism is not clear(Jensen et al., 2012; Labed et al., 2018; Renz et al., 2018). Huperzine A, a selective AChE inhibitor, has been shown to inhibit GSK3α/β activity and enhance the level of

β-catenin in transgenic mouse model of Alzheimer's disease, as well as in cultured SH-SY5Y cells(Wang et al., 2011). In parallel, the application of Donepezil in scopolamine-induced mice showed similar inhibition on the activity of GSK3α/β(Machhi et al., 2016). Nor-galanthamine, an alkaloid and a potent AChE inhibitor, triggered the anagen-activating signalling pathways, including ERK1/2, AKT and β-catenin pathway, in cultured DPC (Yoon et al., 2019). These findings are consistent with our results that the inhibition of AChE in DPC can promote hair growth via activation of AChR and subsequently the Wnt signalling.

In skin, ACh was first identified in 1962 by Scott(Scott, 1962). The functionalities of ACh in skin have been proposed, and one of them is playing a role in skin pigmentation(Arredondo et al., 2003; Wu, Bai, et al., 2020). Keratinocyte and melanocyte form a so called "skin synapse" in the skin epidermis. Keratinocyte is able to release ACh, triggered by light-activated opsin, and that acts on mAChR of melanocyte, as such to regulate the production and release of melanin(Wu et al., 2018; Wu, Xia, et al., 2020). Similar to the situation in skin, the hair DPC could release ACh, possibly triggered by solar light-activated opsins(Bellono et al., 2014; Kelley & Davies, 2016). In contrast, the released ACh is acting as an autocrine to trigger the responses on DPC itself. However, the exact sub-types of opsins in directing this function are not known; but at least the expressions of opsins 1-3 are peaked at first day after DPC culture. Besides, the ACh level is shown to be higher in anagen phase than in telogen phase of hair follicle, which is consistent with the hypothesis that the opsin is interacting with cholinergic molecules via solar light to regulate hair growth.

Although various mAChRs, including M1 to M5, were found in the dermal papilla. Here, we propose M4 mAChR should be the primary target to mediate the cholinergic signalling in hair growth. In line to this notion, M3 and M4 mAChR have

been reported to involve in keratinocyte migration and hair growth cycling. The M4 mAChR knock-out mice displayed retardation of hair follicle morphogenesis(Hasse et al., 2007), and similarly a decreased keratinocyte migration was observed upon transfection with siRNA of M4 mAChR(Chernyavsky et al., 2004). The reciprocal effect was revealed in keratinocyte transfected with siRNA-M3 mAChR and M3 mAChR KO mice(Chernyavsky et al., 2004). In line to these reports, an inhibition of M3 mAChR using 4-DAMP was able to stimulate the Wnt signalling in cultured DPCs, as shown here. Conversely, the inhibition of M4 mAChR using tropicamide or M4 mAChR targeted siRNA can inhibit the Wnt signalling, even in the present of bethanechol. Moreover, with the pretreatment of the non-specific antagonist atropine in DPC, Wnt signalling was inhibited even with the induction of bethanechol. Thus, the inhibitory effect of M4 mAChR on Wnt signalling outweighed the stimulatory effect of M3 mAChR in the presence of atropine. This suggests that the role of M4 mAChR may take higher priority than M3 mAChR.

Materials and Methods

Cell cultures and chemicals

Immortalized DPCs were obtained from Applied Biological Materials (Richmond, BC, Canada). SH-SY5Y cells (a human neuroblastoma line) and Human keratinocyte HaCaT were purchased from American Type Culture Collection (ATCC, Manassas, VA). DPC, SH-SY5Y and HaCaT cells were cultured in Dulbecco's modified Eagle medium supplemented with 10% fetal bovine serum (FBS) and 1% (v/v) penicillin/streptomycin (stock as 10,000 U and 10,000 mg/mL) in 5% CO_2 at 37 °C. Rat pheochromocytoma PC12 cells derived from the rat adrenal medulla were obtained from the American Type Culture Collection (ATCC 1721, Manassas, VA). PC12 cells

were cultured in DMEM supplemented with 6% fetal bovine serum (FBS), 6% horse serum, and 1% penicillin/streptomycin (10,000 U/mL and 10,000 μg/mL). All culture reagents were purchased from Thermo Fisher Scientific (Waltham, MA). The siRNA-M4 was custom synthesized by GenePharma (Shanghai, China). The target sequences for the human *CHRM4* (NM_000741) gene was 5'-CCT CTA CAC CGT GTA CAT C-3' as reported previously(Chernyavsky et al., 2004). The sequence of negative control siRNA was 5'-UUC UCC GAA CGU GUC ACG UTT-3'.

Animals

Animals were obtained from Animal and Plant Care Facility of Hong Kong University of Science and Technology (HKUST) and performed according to the guidelines of Department of Health, The Government of Hong Kong SAR. The experimental procedures were reviewed and approved by Animal Ethics Committee at the University (Reference No.: (15-50) in DH/SHS/8/2/2 Pt.2). Housing was at a constant temperature (21 °C) and humidity (60%), under a fixed 12-hour light/dark cycle and free access to food and water.

DNA transfection and luciferase reporter assay

The plasmid having TCF/LEF-firefly luciferase reporter (pTOPflash) with two repeats, each containing three copies of the TCF-binding site upstream of thymidine kinase minimal promoter, was purchased from Upstate Biotechnology (Lake Placid, NY). The pGloSensor-22F cAMP plasmid was purchased from Promega (Madison, WI). GloSensor™ luciferase contains cAMP binding domain that is fused to a circularly permuted form of firefly luciferase. pCRE-Luc contains CRE promoter sequences with a luciferase reporter, purchased from BD Biosciences. siRNA-M4, 5'-CCT CTA CAC CGT GTA CAT C-3' (corresponding to amino acids 259–279), was custom synthesized

by GenePharm (Shanghai, China), as reported previously(Chernyavsky et al., 2004). The reporter constructs were then transfected using human hair follicle dermal papilla cell (HFDPC) Avalanche® Transfection Reagent (EZ Biosystems, College Park, MD) according to the given instruction. In short, DPC was seeded into 6-well plate incubated overnight in 5% CO_2 at 37°C in a humidified environment without the use of penicillin/streptomycin in the culture medium. After 3 hours incubation with the transfected mixture, the medium was aspirated and replaced by DMEM supplement with 10% FBS and different drug treatment. For the transfection of pGloSensor-22F cAMP plasmid and siRNA-M4, the transfection mixture was incubated overnight. After 24 hours, the cell was collected for the luciferase reporter assay. The luciferase assay was performed using Pierce™ firefly luciferase kit (Thermo Fisher Scientific, Waltham, MA). The luminescent reaction was quantified in a GloMax® 96 microplate luminometer (Thermo Fisher Scientific) and normalized to the total protein. For the pGloSensor-22F cAMP assay, the pre-incubated medium was replaced by fresh medium containing 500 μM of 3-isobutyl-1-methylxanthine and treated with or without drug for 15 min before the addition of 10 μM forskolin. After 15 min of forskolin treatment, the culture was lysed, followed by the luciferase assay.

Sucrose density gradient analysis

Different AChE forms were separated by sucrose density gradient analysis according to previous method(Choi et al., 2008; Xia et al., 2022). In brief, a continuous 5-20% sucrose gradient in lysis buffer containing 10 mM HEPES, pH 7.5, 1 mM EDTA, 1 mM EGTA, 0.2% Triton X-100, and 150 mM NaCl was prepared in a 12-ml polyallomer ultracentrifugation tube. Two hundred μL (1 μg/μL) cell lysates mixed with sedimentation markers, including alkaline phosphatase (6.1 S) and β-galactosidase (16 S), were loaded onto the gradients followed by centrifugation as 38,000 rpm in SW41

Ti Rotor (Beckman, Palo Alto) at 4 °C for 16 hours. Approximately 48 fractions were collected for determination of AChE activity by Ellman assay. In Ellman assay, 0.1 mM tetra-iso-propylpyrophosphoramide (iso-OMPA; Sigma-Aldrich, St Louis, MO), 0.625 mM acetylthiocholine (ATCh; Sigma-Aldrich), and 0.5 mM 5,5-dithiobis-2-nitrobenzoic acid (DTNB) in 80 mM Na_2HPO_4, pH 7.4, was added to the sample. The mixture was incubated at room temperature for 30 min, and AChE activities were measured at 405 nm using Multiskan™ FC microplate photometer. The enzyme activity was expressed as absorbance units/min/g of protein.

Real-time PCR

Total RNA was extracted from cultured DPCs using RNAzol™ Reagent (Sigma-Aldrich), and 3 μg of RNA was reverse transcribed using PrimeScript™ RT reagent kit (Takara, San Jose, CA), according to manufacturer's instruction. Template cDNAs were subjected to RT-PCR using the following specific primers provided in **Supplementary Fig 3.** Real-time PCR was performed in LightCycler 480 (Roche Molecular Biochemical, Indianapolis, IN) using KAPA SYBR FAST qPCR kits in accordance with the manufacturer's instruction. The $2^{\Delta\Delta Ct}$ method was used to calculate the relative expression levels.

Vibrissae culture

Mouse vibrissae were carefully isolated from the upper lip pad of 4-week-old C57BL/6 male mice and cultured in Williams E medium (Sigma-Aldrich), supplemented with 1% (v/v) penicillin/ streptomycin solution, under 5% CO_2 at 37 °C. Five vibrissae were isolated for each group. Vibrissae were incubated in various conditioned medium for 3 days, and the increase in length of hair was measured from days 0 to 3.

Animals and *in vivo* hair growth test

Six-week-old male C57BL/6 mice were chosen for the experiment allowed to adapt to their new environment for 1 week. The hairs on the backs of 7-week-old mice, whose hair follicles were in telogen phase, were shaved with a hair clipper. Various drugs were applied topically daily for up to 14 days. All reagents used for the hair re-growth test were dissolved in a vehicle composed of 100% ethanol and mixed with equal amount of cream.

Skin cryosection preparation

The dorsal skin from C57BL/6 mice was shaved to remove hair and collected after being sacrificed. Skin tissue was fixed with 4% paraformaldehyde for 1h at room temperature and then perfused with 30% sucrose solution in PBS. Afterward, the skin was embedded in OCT and frozen at -80 °C overnight followed by cutting into 30 μm section with Thermo CryoStar NX 70 Cryostat (Thermo Fisher Scientific). The section was preserved at -20 °C for the following experiments.

Immuno-fluorescent staining

Cultured cells were grown on glass coverslips in 35-mm culture dishes. After PBS wash, cells were fixed with 4% paraformaldehyde for 15 min. Cells were incubated with or without 0.1% Triton X-100 in PBS for 10 min and then blocked by 5% BSA for 1 hour. Cultures were stained with primary antibodies for 16 hours at 4 °C, followed with Alexa 488/555/647-conjugated secondary antibodies (Sigma-Aldrich) for 2 hours. The following antibodies were used: anti-AChE at 1:100 (Santa Cruz), anti-BChE at 1:100 (R&D System), anti-M4 mAChR at 1:100 (Abcam Ltd), anti-ChAT at 1:100 (Abcam Ltd), anti-SYP at 1:100 (Santa Cruz), anti-SOX2 at 1:100 (Abcam Ltd), anti-Ki67 at 1:100 (Abcam Ltd). Samples were mounted with ProLong™ Gold antifade mountant with or without DAPI (Thermo Fisher Scientific). Samples were then

examined by Zeiss Celldiscoverer 7 automated microscope (Zeiss, Oberkochen, Germany).

Measurement of ACh

The amount of ACh in conditioned medium or skin tissue from wild-type mice was measured using Acetylcholine ELISA Kit (Colorimetric) (Abcam Ltd) or LC–MS/MS. Briefly, cells were seeded and cultured in a 60-mm culture dish. After 48 hours, the culture medium was replaced by DMEM without FBS supplied with 20 μM BW284c51 and 20 μM iso-OMPA for 30 min. The culture medium was replaced by Ringer's buffer (7.2 g/L NaCl, 0.37 g/L KCl, 0.17 g/L CaCl2, and pH 7.4) with 20 μM BW284c51 and 20 μM iso-OMPA, then cells were exposed under the solar light simulator machine (Newport Corporation, Irvine, CA) or treated with KCl. The experimental irradiance contained UVA (0.5 mW/m2), UVB (50 mW/m2), and UVC (50 mW/m^2). The Ringer's buffer containing ACh, released by cells, was collected, heated at 55 °C for 5 min to deactivate cholinesterase and concentrated with freeze drying, followed by ACh assay performed. In brief, the amount of choline in each sample was determined using the probe for choline before and after adding AChE. The amount of ACh was acquired by subtracting the amount of choline before adding AChE from that after adding AChE. For the ACh amount in the skin tissue, the mouse skin tissue was heated with 55 °C for 5 min to deactivate cholinesterase immediately after dissection in lysis buffer containing 10 mM HEPES, pH 7.5, 1 mM EDTA, 1 mM EGTA, 0.2% Triton X-100, and 150 mM NaCl. The samples were then homogenized, vortex and centrifuge to obtain the extract. For LC-MS/MS analysis, LC-MS/MS analysis was conducted an Agilent 6410B triple quadrupole mass spectrometer (QQQ-MS/MS) with ESI source (Agilent Technologies, Waldbronn, Germany) coupled with Agilent 1290 Infinity Binary Liquid Chromatography Systems. Chromatographic separation was achieved on

a PC HILIC (150mm×2 mm, 3 μm, Osaka Soda, Osaka, Japan) at 35 °C. For conditioned medium, after freeze drying, the solid obtained was redissolved in 100% acetonitrile before injection into the mass spectrometer. For tissue sample, an equal amount of acetonitrile was added to the sample to precipitate the protein before injecting into the mass spectrometer. The mobile phase consisted of water containing 20 mM ammonium formate and 0.2% formic acid (A) and acetonitrile containing 0.1% formic acid (B) at a flow rate of 0.4 ml/min. The gradient elution was programmed as follows: 0–2 min, 2% A; 2-2.01 min, 2-25% A; 2.01–4 min, 25% A; 4–5 min, 25-50% A; 5-8 min, 50% A; 8–10 min; 50-2% A and 10-13 min, 2% A.

Statistical analysis

Each result is represented as the mean ± SEM, calculated from independent replicates. Comparisons of the means for untreated control cells and treated cells were analysed using Student's *t*-test. Significant values were represented as $*p < 0.05$, $**p < 0.01$, $***p < 0.001$.

Acknowledgments

Funding: This work is supported by supported by Hong Kong Research Grants Council Hong Kong (GRF 16100921); Zhongshan Municipal Bureau of Science and Technology (2019AG035); Guangzhou Science and Technology Committee Research Grant (GZSTI16SC02; GZSTI17SC02); GBA Institute of Collaborate Innovation (GICI-022); The Key-Area Research and Development Program of Guangdong Province (2020B1111110006)；Special project of Foshan University of Science and Technology in 2019 (FSUST19-SRI10); Hong Kong RGC Theme-based Research Scheme (T13-605/18-W); Hong Kong Innovation Technology Fund (ITS/500/18FP;

MHP/004/21; GHP/016/21SZ; ITCPD/17-9; ITC-CNERC14SC01); TUYF19SC02, PD18SC01 and HMRF18SC06; HMRF20SC07, AFD20SC01; Shenzhen Science and Technology Innovation Committee (ZDSYS201707281432317).

Author contributions:

G.K.W.Y., Conceptualization, Methodology, Investigation, Visualization, Writing—original draft, Writing—review & editing; K.W.L., Methodology, Investigation; S.Y.J.X., Methodology; K.Q.Y.W., Investigation; A.X.G, Investigation; Q.W.S.L., Investigation; J.Y.M.H., Software H.C.T.C., Investigation; M.S.S.G., Investigation; K.W.K.T., Supervision, Writing—review & editing.

Declaration of interests:

The authors declare no competing interests.

Data and materials availability:

All data needed to evaluate the conclusions in the paper are present in the paper and/or the Supplementary Materials.

References

Andl T, Reddy ST, Gaddapara T, Millar SE. 2002. WNT signals are required for the initiation of hair follicle development. *Developmental cell* **2**:643-653. DOI: https://doi.org/10.1016/s1534-5807(02)00167-3.

Arredondo J, Hall LL, Ndoye A, Nguyen VT, Chernyavsky AI, Bercovich D, Orr-Urtreger A, Beaudet AL, Grando SA. 2003. Central role of fibroblast α3 nicotinic acetylcholine receptor in mediating cutaneous effects of nicotine. *Laboratory Investigation* **83**:207-225. DOI: https://doi.org/10.1097/01.lab.0000053917.46614.12.

Beaudoin III GM, Sisk JM, Coulombe PA, Thompson CC. 2005. Hairless triggers reactivation of hair growth by promoting Wnt signaling. *Proceedings of the National Academy of Sciences* **102**:14653-14658. DOI: https://doi.org/10.1073/pnas.0507609102.

Beckmann J, Lips KS. 2013. The non-neuronal cholinergic system in health and disease. *Pharmacology* **92**:286-302. DOI: https://doi.org/10.1159/000355835.

Bellono NW, Najera JA, Oancea E. 2014. UV light activates a Gαq/11-coupled phototransduction pathway in human melanocytes. *Journal of General Physiology* **143**:203-214. DOI: https://doi.org/10.1085/jgp.201311094.

533 Bernard BA. 2006. La vie révélée du follicule de cheveu humain. *médecine/sciences* **22**:138-
534 143. DOI: https://doi.org/10.1051/medsci/2006222138.

535 Chan LKM, Braidy N, Ng W, Xu YH, Chen J, McDonald R, Chan DKY. 2020. Re-pigmentation of
536 hair after prolonged cholinesterase inhibitor therapy in a Chinese population.
537 *Australasian Journal of Dermatology* **61**:417-420. DOI: https://doi.org/10.1111/ajd.13356.

538 Chernyavsky AI, Arredondo J, Wess Jr, Karlsson E, Grando SA. 2004. Novel signaling pathways
539 mediating reciprocal control of keratinocyte migration and wound epithelialization
540 through M3 and M4 muscarinic receptors. *The Journal of cell biology* **166**:261-272. DOI:
541 https://doi.org/10.1083/jcb.200401034.

542 Choi RC, Mok MK, Cheung AW, Siow NL, Xie HQ, Tsim KW. 2008. Regulation of PRiMA-linked
543 G4 AChE by a cAMP-dependent signaling pathway in cultured rat pheochromocyoma
544 PC12 cells. *Chemico-biological interactions* **175**:76-78. DOI:
545 https://doi.org/10.1016/j.cbi.2008.04.007.

546 Driskell RR, Clavel C, Rendl M, Watt FM. 2011. Hair follicle dermal papilla cells at a glance.
547 *Journal of cell science* **124**:1179-1182. DOI: https://doi.org/10.1242/jcs.082446.

548 Grando SA. 2007. Recent progress in understanding the non-neuronal cholinergic system in
549 humans. *Life sciences* **80**:2181-2185. DOI: https://doi.org/10.1016/j.lfs.2007.03.015

550 Grando SA, Kist DA, Qi M, Dahl MV. 1993. Human keratinocytes synthesize, secrete, and
551 degrade acetylcholine. *Journal of Investigative Dermatology* **101**:32-36. DOI:
552 https://doi.org/10.1111/1523-1747.ep12363399.

553 Guo MS, Wu Q, Dong TT, Tsim KWK. 2023. The UV-induced uptake of melanosome by skin
554 keratinocyte is triggered by α7 nicotinic acetylcholine receptor-mediated phagocytosis.
555 *The FEBS journal* **290**:724-744. DOI: https://doi.org/10.1111/febs.16613.

556 Hasse S, Chernyavsky AI, Grando SA, Paus R. 2007. The M4 muscarinic acetylcholine receptor
557 plays a key role in the control of murine hair follicle cycling and pigmentation. *Life*
558 *sciences* **80**:2248-2252. DOI: https://doi.org/10.1016%2Fj.lfs.2007.01.056.

559 Heyer G, Vogelgsang M, Hornstein OP. 1997. Acetylcholine is an inducer of itching in patients
560 with atopic eczema. *The Journal of dermatology* **24**:621-625. DOI:
561 https://doi.org/10.1111/j.1346-8138.1997.tb02305.x

562 Hibino T, Nishiyama T. 2004. Role of TGF-β2 in the human hair cycle. *Journal of*
563 *dermatological science* **35**:9-18. DOI: https://doi.org/10.1016/j.jdermsci.2003.12.003

564 Huelsken J, Vogel R, Erdmann B, Cotsarelis G, Birchmeier W. 2001. β-Catenin controls hair
565 follicle morphogenesis and stem cell differentiation in the skin. *Cell* **105**:533-545. DOI:
566 https://doi.org/10.1016/s0092-8674(01)00336-1.

567 Imbernón-Moya A, Podlipnik S, Burgos F, Vargas-Laguna E, Aguilar-Martínez A, Fernández-
568 Cogolludo E, Gallego-Valdes MA. 2016. Acquired localized hypertrichosis induced by
569 rivastigmine. *Case reports in dermatological medicine* **2016**:7296572-7296573. DOI:
570 https://doi.org/10.1155/2016/7296572.

571 Jensen M, Hoerndli FJ, Brockie PJ, Wang R, Johnson E, Maxfield D, Francis MM, Madsen DM,
572 Maricq AV. 2012. Wnt signaling regulates acetylcholine receptor translocation and
573 synaptic plasticity in the adult nervous system. *Cell* **149**:173-187. DOI:
574 https://doi.org/10.1016%2Fj.cell.2011.12.038.

575 Kelley JL, Davies WI. 2016. The biological mechanisms and behavioral functions of opsin-
576 based light detection by the skin. *Frontiers in ecology and evolution* **4**:106. DOI:
577 https://doi.org/10.3389/fevo.2016.00106.

578 Kishimoto J, Burgeson RE, Morgan BA. 2000. Wnt signaling maintains the hair-inducing
579 activity of the dermal papilla. *Genes & development* **14**:1181-1185. DOI:
580 https://www.ncbi.nlm.nih.gov/pmc/articles/PMC316619/.

581 Kowal NM, Ahring PK, Liao VW, Indurti DC, Harvey BS, O'Connor SM, Chebib M, Olafsdottir
582 ES, Balle T. 2018. Galantamine is not a positive allosteric modulator of human α4β2 or α7
583 nicotinic acetylcholine receptors. *British journal of pharmacology* **175**:2911-2925. DOI:
584 https://doi.org/10.1111/bph.14329.

585 Kurzen H, Wessler I, Kirkpatrick C, Kawashima K, Grando S. 2007. The non-neuronal
586 cholinergic system of human skin. *Hormone and metabolic research* **39**:125-135. DOI:
587 https://doi.org/10.1055/s-2007-961816.

588 Labed SA, Wani KA, Jagadeesan S, Hakkim A, Najibi M, Irazoqui JE. 2018. Intestinal epithelial
589 Wnt signaling mediates acetylcholine-triggered host defense against infection. *Immunity*
590 **48**:963-978. DOI: https://doi.org/10.1016/j.immuni.2018.04.017.

591 Lin W-h, Xiang L-J, Shi H-X, Zhang J, Jiang L-p, Cai P-t, Lin Z-L, Lin B-B, Huang Y, Zhang H-L.
592 2015. Fibroblast growth factors stimulate hair growth through β-catenin and Shh
593 expression in C57BL/6 mice. *BioMed research international* **2015**:139-730. DOI:
594 https://doi.org/10.1155/2015/730139.

595 Lin X, Zhu L, He J. 2022. Morphogenesis, growth cycle and molecular regulation of hair
596 follicles. *Frontiers in cell and developmental biology* **10**:899095-899096. DOI:
597 https://doi.org/10.3389/fcell.2022.899095.

598 Machhi J, Sinha A, Patel P, Kanhed AM, Upadhyay P, Tripathi A, Parikh ZS, Chruvattil R, Pillai
599 PP, Gupta S. 2016. Neuroprotective potential of novel multi-targeted isoalloxazine
600 derivatives in rodent models of Alzheimer's disease through activation of canonical
601 Wnt/β-catenin signalling pathway. *Neurotoxicity research* **29**:495-513. DOI:
602 https://doi.org/10.1007/s12640-016-9598-4.

603 Matsuzaki T, Yoshizato K. 1998. Role of hair papilla cells on induction and regeneration
604 processes of hair follicles. *Wound Repair and Regeneration* **6**:524-530. DOI:
605 https://doi.org/10.1046/j.1524-475x.1998.60605.x.

606 McGleenon B, Dynan K, Passmore A. 1999. Acetylcholinesterase inhibitors in Alzheimer's
607 disease. *British journal of clinical pharmacology* **48**:471-472. DOI:
608 https://doi.org/10.1046/j.1365-2125.1999.00026.x.

609 Morgan BA. 2014. The dermal papilla: an instructive niche for epithelial stem and progenitor
610 cells in development and regeneration of the hair follicle. *Cold Spring Harbor perspectives*
611 *in medicine* **4**:15180-15181. DOI: https://doi.org/10.1101%2Fcshperspect.a015180.

612 Müller T. 2007. Rivastigmine in the treatment of patients with Alzheimer's disease.
613 *Neuropsychiatric Disease and Treatment* **3**:211-218. DOI:
614 https://doi.org/10.2147%2Fnedt.2007.3.2.211

615 Natarelli N, Gahoonia N, Sivamani RK. 2023. Integrative and Mechanistic Approach to the
616 Hair Growth Cycle and Hair Loss. *Journal of clinical medicine* **12**:893-894. DOI:
617 https://doi.org/10.3390%2Fjcm12030893.

618 Oh JW, Kloepper J, Langan EA, Kim Y, Yeo J, Kim MJ, Hsi T-C, Rose C, Yoon GS, Lee S-J. 2016. A
619 guide to studying human hair follicle cycling in vivo. *Journal of Investigative Dermatology*
620 **136**:34-44. DOI: https://doi.org/10.1038/jid.2015.354.

621 Paus R, Cotsarelis G. 1999. The biology of hair follicles. *New England journal of medicine*
622 **341**:491-497. DOI: https://doi.org/10.1056/NEJM199908123410706.

623 Prvulovic D, Hampel H, Pantel J. 2010. Galantamine for Alzheimer's disease. *Expert opinion*
624 *on drug metabolism & toxicology* **6**:345-354. DOI:
625 https://doi.org/10.1517/17425251003592137.

626 Rendl M, Polak L, Fuchs E. 2008. BMP signaling in dermal papilla cells is required for their hair
627 follicle-inductive properties. *Genes & development* **22**:543-557. DOI:
628 https://doi.org/10.1101/gad.1614408.

629 Renz BW, Tanaka T, Sunagawa M, Takahashi R, Jiang Z, Macchini M, Dantes Z, Valenti G, White
630 RA, Middelhoff MA. 2018. Cholinergic Signaling via Muscarinic Receptors Directly and
631 Indirectly Suppresses Pancreatic Tumorigenesis and Cancer Stemness Cholinergic
632 Signaling Suppresses Pancreatic Tumorigenesis. *Cancer discovery* **8**:1458-1473. DOI:
633 https://doi.org/10.1158/2159-8290.cd-18-0046.

634 Scott A. 1962. Acetylcholine in normal and diseased skin. *British Journal of Dermatology*
635 **74**:317-322. DOI: https://doi.org/10.1111/j.1365-2133.1962.tb13518.x.

636 Scott LJ, Goa KL. 2000. Galantamine: a review of its use in Alzheimer's disease. *Drugs*
637 **60**:1095-1122. DOI: https://doi.org/10.2165/00003495-200060050-00008.

638 Sharov AA, Fessing M, Atoyan R, Sharova TY, Haskell-Luevano C, Weiner L, Funa K, Brissette
639 JL, Gilchrest BA, Botchkarev VA. 2005. Bone morphogenetic protein (BMP) signaling
640 controls hair pigmentation by means of cross-talk with the melanocortin receptor-1
641 pathway. *Proceedings of the National Academy of Sciences* **102**:93-98. DOI:
642 https://doi.org/10.1073/pnas.0408455102.

643 Takahashi T. 2021. Multiple roles for cholinergic signaling from the perspective of stem cell
644 function. *International journal of molecular sciences* **22**:666-667. DOI:
645 https://doi.org/10.3390/ijms22020666.

646 Van der Westhuizen ET, Choy KC, Valant C, McKenzie-Nickson S, Bradley SJ, Tobin AB, Sexton
647 PM, Christopoulos A. 2021. Fine tuning muscarinic acetylcholine receptor signaling
648 through allostery and bias. *Frontiers in pharmacology* **11**:606656-606657. DOI:
649 https://doi.org/10.3389/fphar.2020.606656.

650 Vecchio I, Sorrentino L, Paoletti A, Marra R, Arbitrio M. 2021. The state of the art on
651 acetylcholinesterase inhibitors in the treatment of Alzheimer's disease. *Journal of central*
652 *nervous system disease* **13**:11795735211029113. DOI:
653 https://doi.org/10.1177%2F11795735211029113.

654 Wang C-Y, Zheng W, Wang T, Xie J-W, Wang S-L, Zhao B-L, Teng W-P, Wang Z-Y. 2011.
655 Huperzine A activates Wnt/β-catenin signaling and enhances the nonamyloidogenic
656 pathway in an Alzheimer transgenic mouse model. *Neuropsychopharmacology* **36**:1073-
657 1089. DOI: https://doi.org/10.1038/npp.2010.245.

658 Wessler I, Kirkpatrick C. 2008. Acetylcholine beyond neurons: the non-neuronal cholinergic
659 system in humans. *British journal of pharmacology* **154**:1558-1571. DOI:
660 https://doi.org/10.1038/bjp.2008.185.

661 Wessler I, Reinheimer T, Kilbinger H, Bittinger F, Kirkpatrick CJ, Saloga J, Knop J. 2003.
662 Increased acetylcholine levels in skin biopsies of patients with atopic dermatitis. *Life*
663 *sciences* **72**:2169-2172. DOI: https://doi.org/10.1016/S0024-3205(03)00079-1

664 Wu Q, Bai P, Xia Y, Lai QW, Guo MS, Dai K, Zheng Z, Ling CS, Dong TT, Pi R. 2020. Solar light
665 induces expression of acetylcholinesterase in skin keratinocytes: Signalling mediated by
666 activator protein 1 transcription factor. *Neurochemistry international* **141**:104861. DOI:
667 https://doi.org/10.1016/j.neuint.2020.104861.

668 Wu Q, Fung AH, Xu ML, Poon K, Liu EY, Kong XP, Yao P, Xiong QP, Dong TT, Tsim KW. 2018.
669 Microphthalmia-associated transcription factor up-regulates acetylcholinesterase
670 expression during melanogenesis of murine melanoma cells. *Journal of Biological*
671 *Chemistry* **293**:14417-14428. DOI: https://doi.org/10.1074/jbc.RA118.003729.

672 Wu Q, Xia Y, Dai K, Bai P, Kwan KK, Guo MS, Dong TT, Tsim KW. 2020. Solar light induces the
673 release of acetylcholine from skin keratinocytes affecting melanogenesis. *The FASEB*
674 *Journal* **34**:8941-8958. DOI: https://doi.org/10.1016/j.neuint.2020.104861.

675 Xia Y, Wu Q, Mak S, Liu EY, Zheng BZ, Dong TT, Pi R, Tsim KW. 2022. Regulation of
676 acetylcholinesterase during the lipopolysaccharide-induced inflammatory responses in
677 microglial cells. *The FASEB Journal* **36**:22189-22190. DOI:
678 https://doi.org/10.1096/fj.202101302RR.

679 Yang C-C, Cotsarelis G. 2010. Review of hair follicle dermal cells. *Journal of dermatological*
680 *science* **57**: 2-11. DOI: https://doi.org/10.1016/j.jdermsci.2009.11.005.

681 Yano K, Brown LF, Detmar M. 2001. Control of hair growth and follicle size by VEGF-mediated
682 angiogenesis. *The Journal of clinical investigation* **107**: 409-417. DOI:
683 https://doi.org/10.1172%2FJCI11317.

684 Yoon H-S, Kang J-I, Kim SM, Ko A, Koh Y-S, Hyun J-W, Yoon S-P, Ahn MJ, Kim YH, Kang J-H.
685 2019. Norgalanthamine stimulates proliferation of dermal papilla cells via anagen-
686 activating signaling pathways. *Biological and Pharmaceutical Bulletin* **42**: 139-143. DOI:
687 https://doi.org/10.1248/bpb.b18-00226.

688
689
690

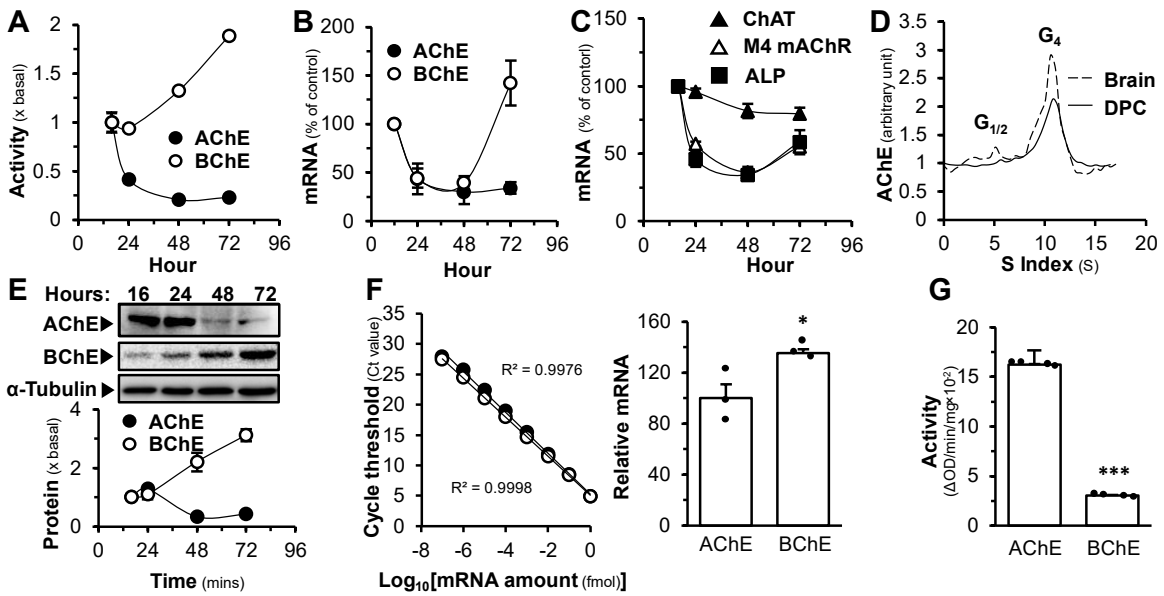

Figure 1. Expression of cholinergic molecules in DPC.

Cultured DPCs were harvested on different days, and cell lysate and mRNA were collected. **(A):** AChE and BChE activities were determined. **(B):** mRNA levels of AChE and BChE. **(C):** mRNA levels of ChAT, M4 mAChR and ALP. **(D):** AChE molecular forms in a sucrose density gradient analysis. The sedimentation (S) value was estimated from the position of the sedimentation markers. **(E):** cell lysates (20 μg) were subjected to Western blot analysis. AChE (~70 kDa), BChE (~ 40 kDa), α-tubulin (~50 kDa; a loading control) are shown (upper) and quantified (lower). **(F):** The standard curve of AChE and BChE mRNA levels was obtained by quantitative PCR (left). The mRNA levels of AChE and BChE in DPC cultures were determined by the absolute quantitative PCR (right). **(G):** The activities of AChE and BChE in DPC cultures were determined. Data are normalized and expressed as the % increase, or % of control, or fold of basal (x basal), or in relative amount in comparison to control, in mean ± SEM (n = 3-4), * $p < 0.05$, ** $p < 0.01$, *** $p < 0.001$.

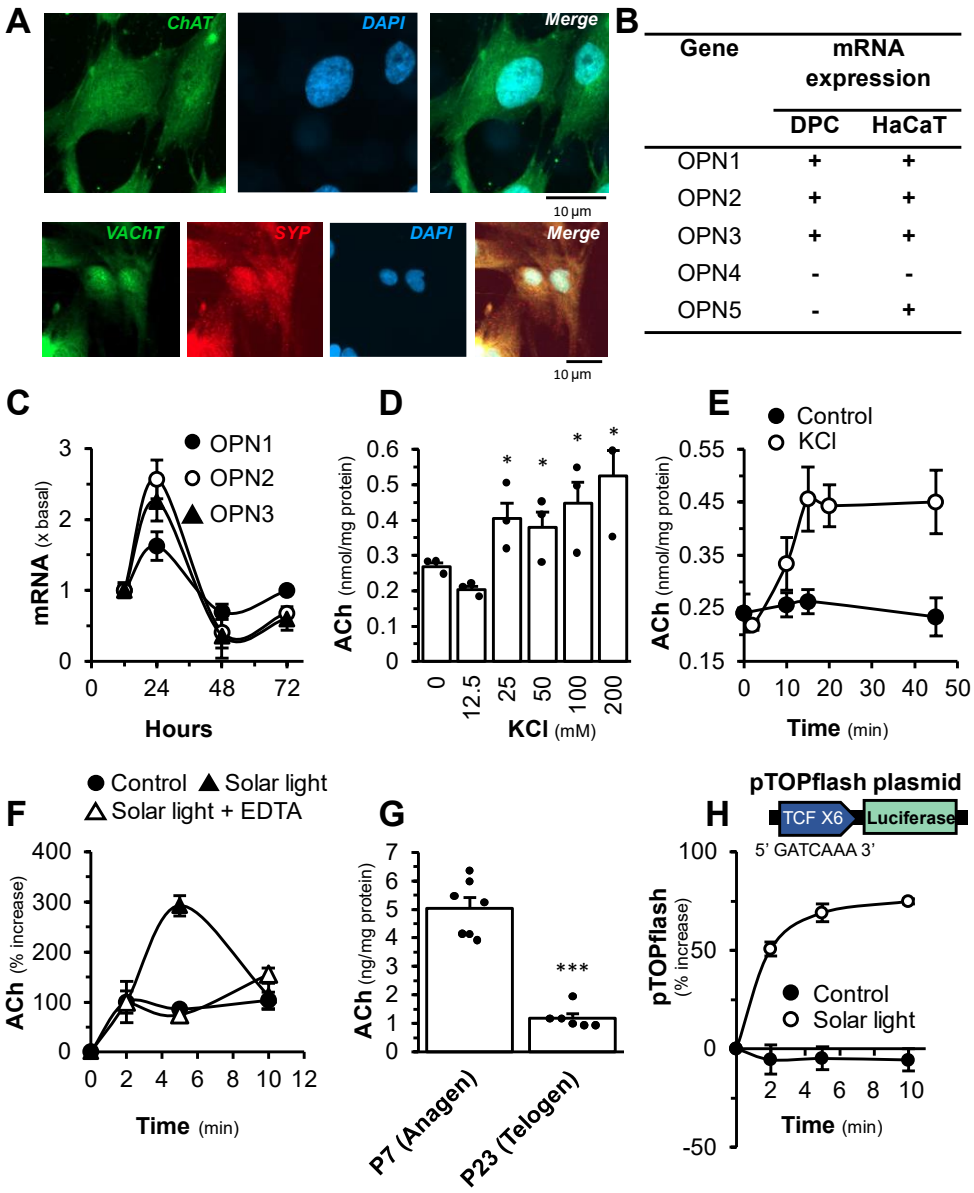

Gene	mRNA expression	
	DPC	HaCaT
OPN1	+	+
OPN2	+	+
OPN3	+	+
OPN4	-	-
OPN5	-	+

Figure 2. Solar light induces the release of ACh from DPC.
(A): Immunocytochemical staining of ChAT (green), VAChT (green), SYP (red) and DAPI staining (blue) in DPC. **(B):** Summary of mRNA expression of opsins in DPC. **(C):** mRNA of OPN1, OPN2, OPN3 of cultured DPC harvested on different days. **(D):** ACh release from DPC with various concentrations of KCl, measured by ELISA at 5 min. **(E):** ACh release from DPC over time with 100 mM KCl, measured by ELISA. **(F):** ACh release from DPC over time with the treatment of solar light with or without EDTA (10 mM), measured by LC-MS/MS analysis. **(G):** ACh levels from skin of wild-type mice in anagen (P7) or telogen (P23), measured by LC-MS/MS analysis, normalized by the protein concentration. **(H):** The luciferase activity assay of pTOPflash-transfected DPC was performed after 6 hours of exposure to solar light for various durations. Data are normalized and expressed as the fold of basal value, in comparison to control, in mean ± SEM (n = 3-6), * $p < 0.05$, ** $p < 0.01$.

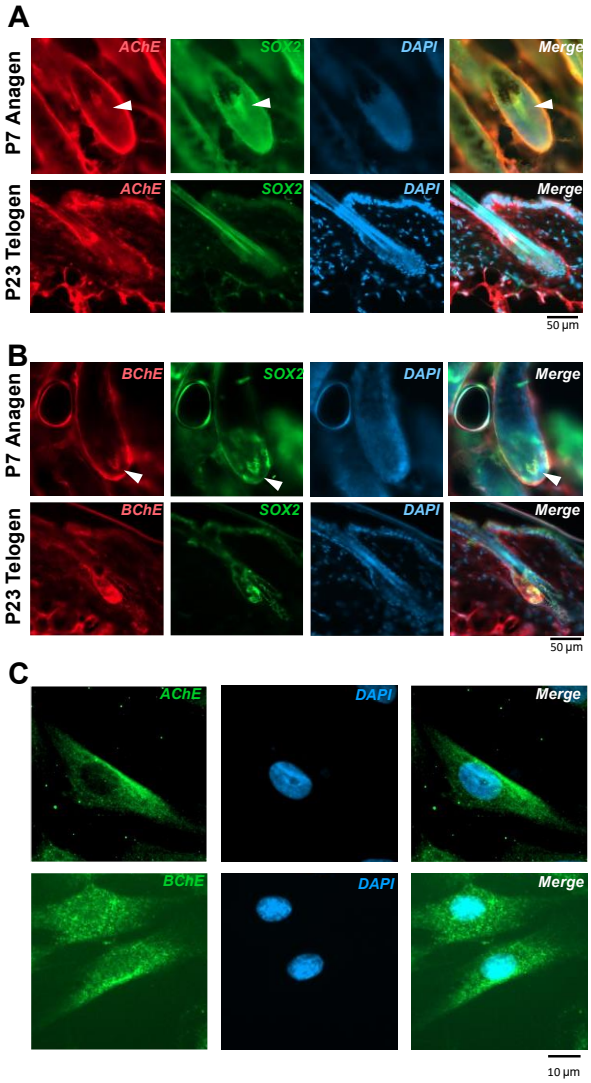

Figure 3. The immunostaining of AChE and BChE in skin from wild-type mice and DPC culture. (A): Skin from wild-type mice in anagen (P7), telogen (P23) was harvested, fixed, and stained with anti-AChE. **(B):** Skin from wild-type mice in anagen (P7), telogen (P23) was harvested, fixed, and stained with anti-BChE. **(C):** Immunocytochemical staining of AChE (green), BChE (green) and DAPI staining (blue) in DPC, *n*=4.

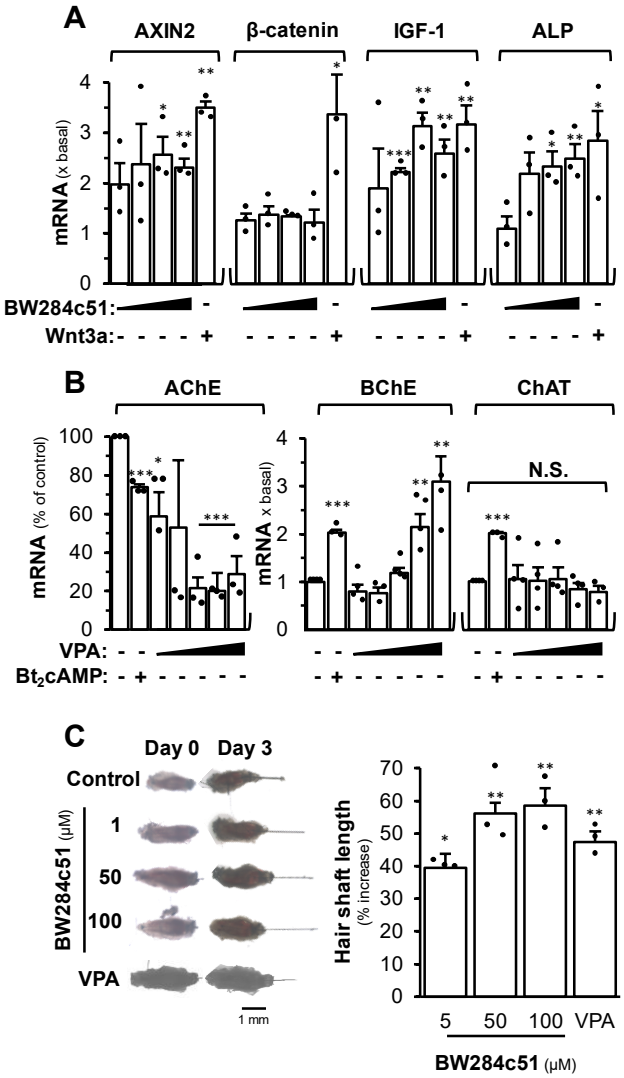

Figure 4. Inhibition of AChE promotes hair growth.
(A): Cultured DPC was treated with different doses of BW284c51 (25, 50, 100 and 200 µM, as indicated), or Wnt3a (200 ng/mL) 48 hours. mRNA levels of AXIN2, LEF-1, β-catenin, IGF-1, and ALP are shown. **(B):** Cultured DPC was treated with different doses of VPA (312, 625, 1250, 2500 and 5,000 µM, as indicated), or Bt_2cAMP (1 mM). mRNA levels of AChE, BChE, ChAT are shown. **(C):** Individual anagen vibrissae were isolated from the upper lip pad of 4-week-old C57BL/6 male mice. The gross image of cultures treated with different doses of BW284c51, or VPA (5 mM) were taken, as indicated for 3 days (left). The measurement of hair shaft elongation was performed (right). Data are normalized and expressed as the % increase, or fold of basal value, in comparison to control, in mean ± SEM, $n = 4$, * $p < 0.05$, ** $p < 0.01$, *** $p < 0.001$.

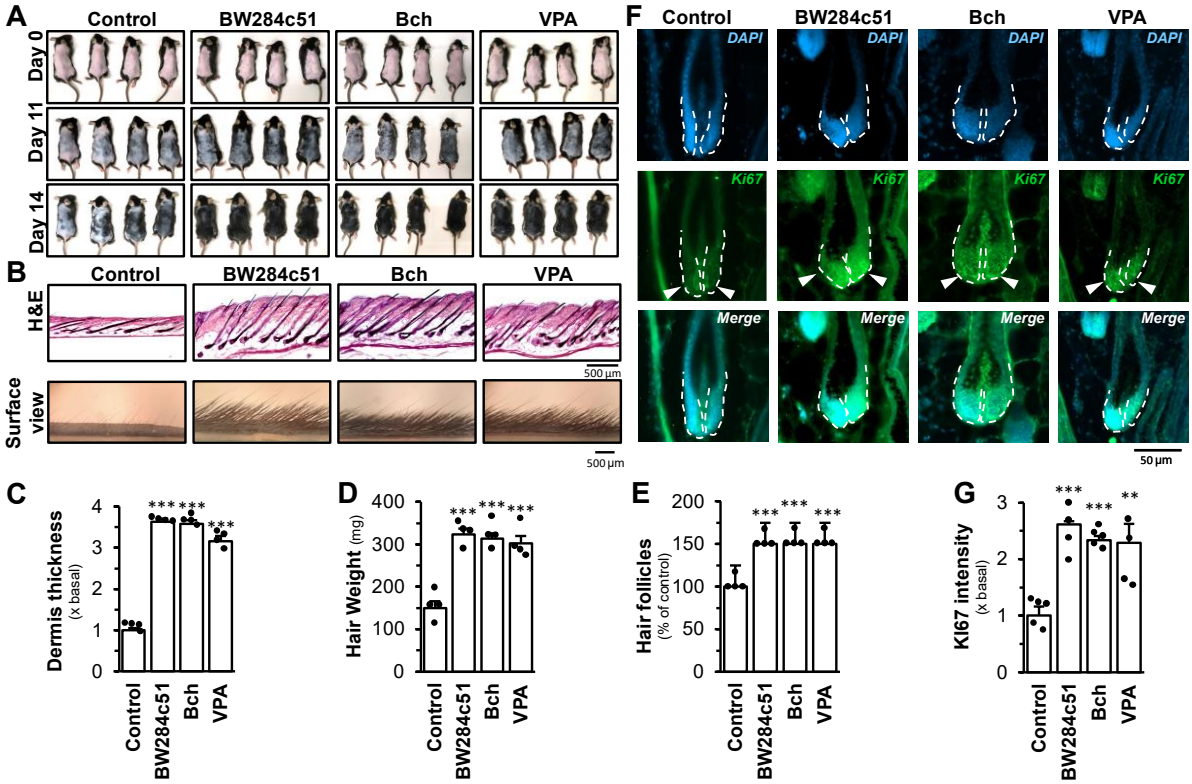

Figure 5. Topical effect of cholinergic drugs accelerated the re-entry of anagen in wild-type mice.

Seven weeks old wild-type mice were shaved and treated daily with either topical application of vehicle control, BW284c51 (200 µM), bethanechol (25 mM), VPA (500 mM). **(A):** Representative gross image of the dorsal back of the mice taken at day 0, 11 and 14. **(B):** Skin was harvested after 14 days and stained with hematoxylin and eosin (H&E) (upper). Surface view shows the status of hair shaft of different treatment (lower). Measurements of **(C):** dermis thickness, **(D):** hair weight, **(E):** hair follicle number of mouse skin corresponding to different treatments from (A). **(F):** Immuno-histochemical staining of Ki67 in the hair bulbs of the skin from mice corresponding to different treatments in (A). **(G):** Quantitative analyses of immunohistochemical staining of Ki67 shown in (F). Data are normalized and expressed as the % of control, or fold of basal value, in comparison to control, in mean ± SEM (n = 4-5), * $p < 0.05$, ** $p < 0.01$, *** $p < 0.001$.

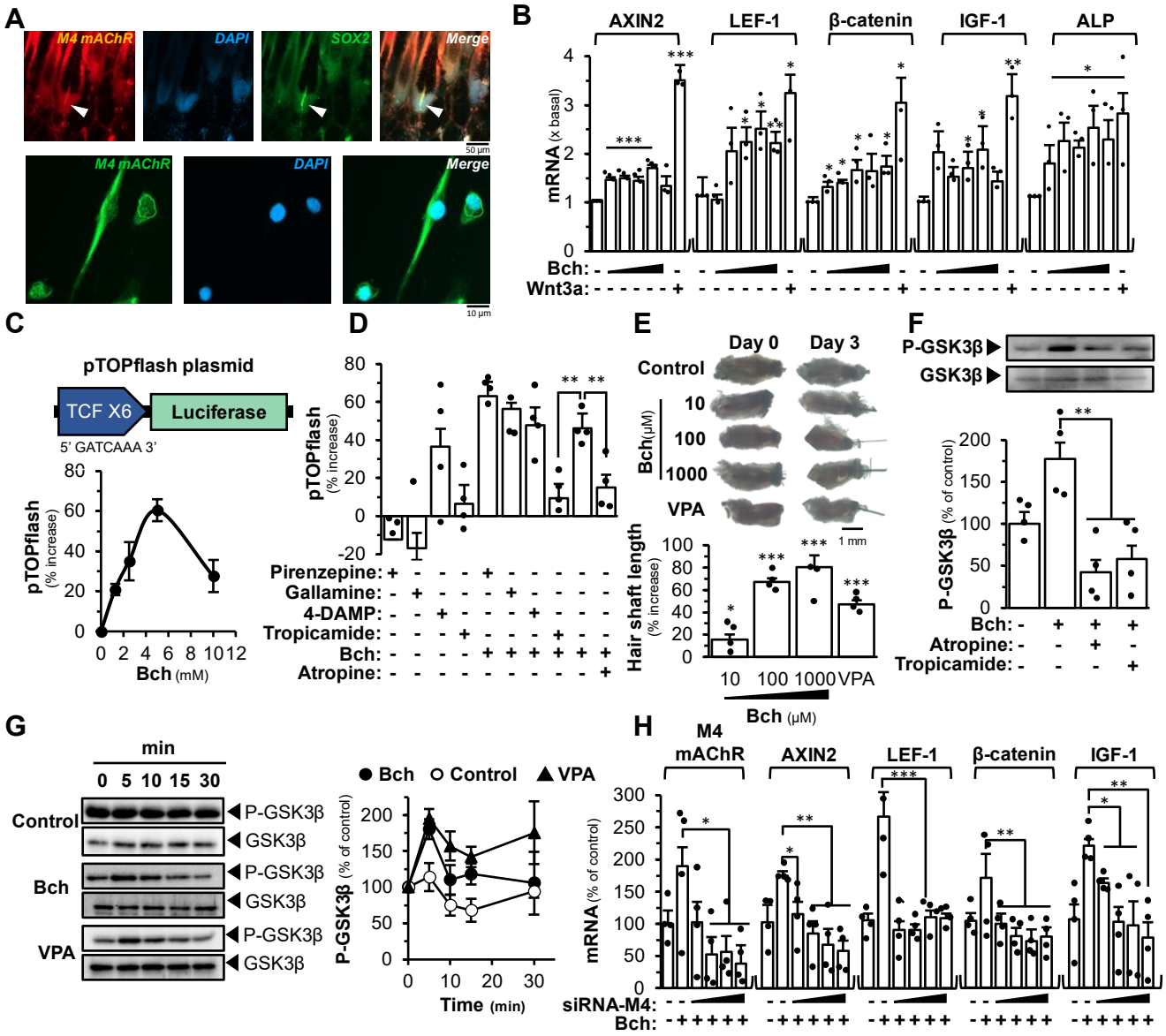

Figure 6. Activation of M4 mAChR promotes hair growth through Wnt signalling.

(A): Immunohistochemical staining of M4 mAChR (red), DAPI staining (blue), SOX2 (green) in the skin section from wild-type mice in anagen (P7) (upper). Immunocytochemical staining of M4 mAChR (red) and DAPI staining (blue) in DPC (lower). Arrowhead indicates dermal papilla. **(B):** Cultured DPC was treated with different doses of bethanechol (312, 625, 1250, 2500 and 5,000 μM, as indicated), or Wnt3a (200 ng/mL), were applied for 48 hours. mRNA levels of AXIN2, LEF-1, β-catenin, IGF-1, and ALP are shown. **(C):** The luciferase activity assay of pTOPflash-transfected DPC treated with different doses of bethanechol for 24 hours. **(D):** The luciferase activity assay of pTOPflash-transfected DPC pre-treated, or treated alone, with pirenzepine (200 μM), or gallamine (200 μM), or 4-DAMP (200 μM), or tropicamide (200 μM), or atropine (50 μM) for 30 min before bethanechol (5 mM) for 24 hours. **(E):** The gross image of individual anagen vibrissae treated with different doses of bethanechol, or VPA (5 mM) for 3 days were taken (upper). The measurement of hair shaft elongation was performed (lower). **(F):** Western blot analyses of phosphorylated GSK3β (P-GSK3β) and total GSK3β from DPC treated with bethanechol (5 mM), or VPA (5 mM), for 5 min, or preincubation with atropine (50

μM) or tropicamide (200 μM) for 30 min. **(G):** Western blot analyses of phosphorylated GSK3β (P-GSK3β) and total GSK3β from DPC which were subjected to bethanechol (5 mM) or VPA (5 mM) incubation for different times as indicated. **(H):** Different doses of siRNA-M4 (1.25, 2.5, 5, 10 nM, as indicated) were transfected in DPC. The siRNA-M4 transfected DPC were treated with or without bethanechol (5 mM) for 24 hours. mRNA of AXIN2, LEF-1, β-catenin, IGF-1, and ALP are shown. Data are normalized and expressed as the % increase, % of control, or fold of basal value, in comparison to control, in mean ± SEM (n = 3-4), * $p < 0.05$, ** $p < 0.01$, *** $p < 0.001$.

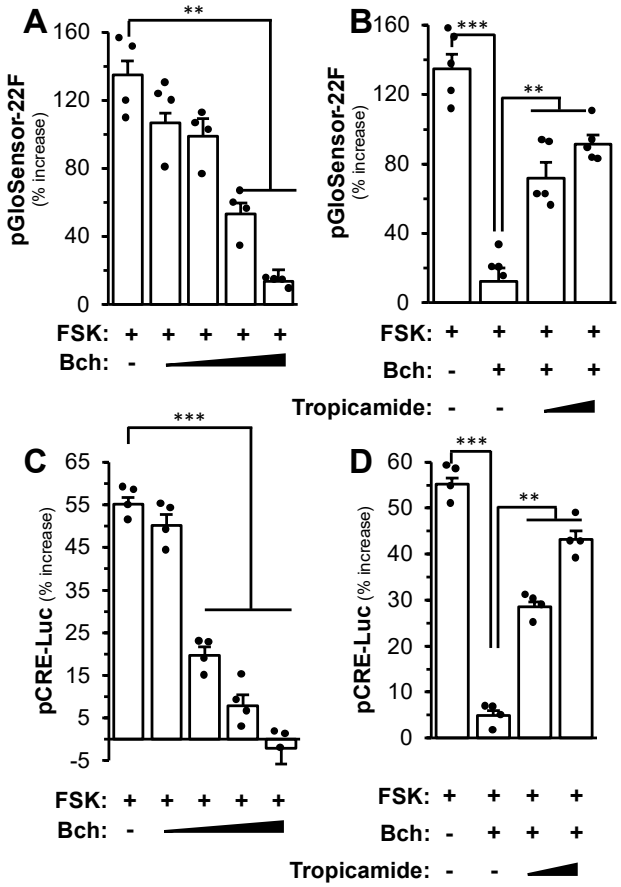

Figure 7. Bethanechol decreases cAMP level in DPC.
(A): The luciferase activity assay of pGloSensor-22F-transfected DPC treated with different concentration of bethanechol (Bch; 1.25, 2.5, 5, 10 mM, as indicated) in the presence of forskolin (FSK; 10 µM). **(B):** The luciferase activity assay of pGloSensor-22F-transfected DPC treated with bethanechol (10 mM) in the presence of forskolin (10 µM), either with or without tropicamide (250 or 500 µM). **(C):** The luciferase activity assay of pCRE-Luc-transfected DPC treated with different concentration of bethanechol (1.25, 2.5, 5, 10 mM, as indicated) in the presence of forskolin (10 µM). **(D):** The luciferase activity assay of pCRE-Luc-transfected DPC treated with bethanechol (10 mM) in the presence of forskolin (10 µM), either with or without tropicamide (250 or 500 µM). Data are normalized and expressed as the % increase in comparison to control, in mean ± SEM (n = 4), ** $p < 0.01$.

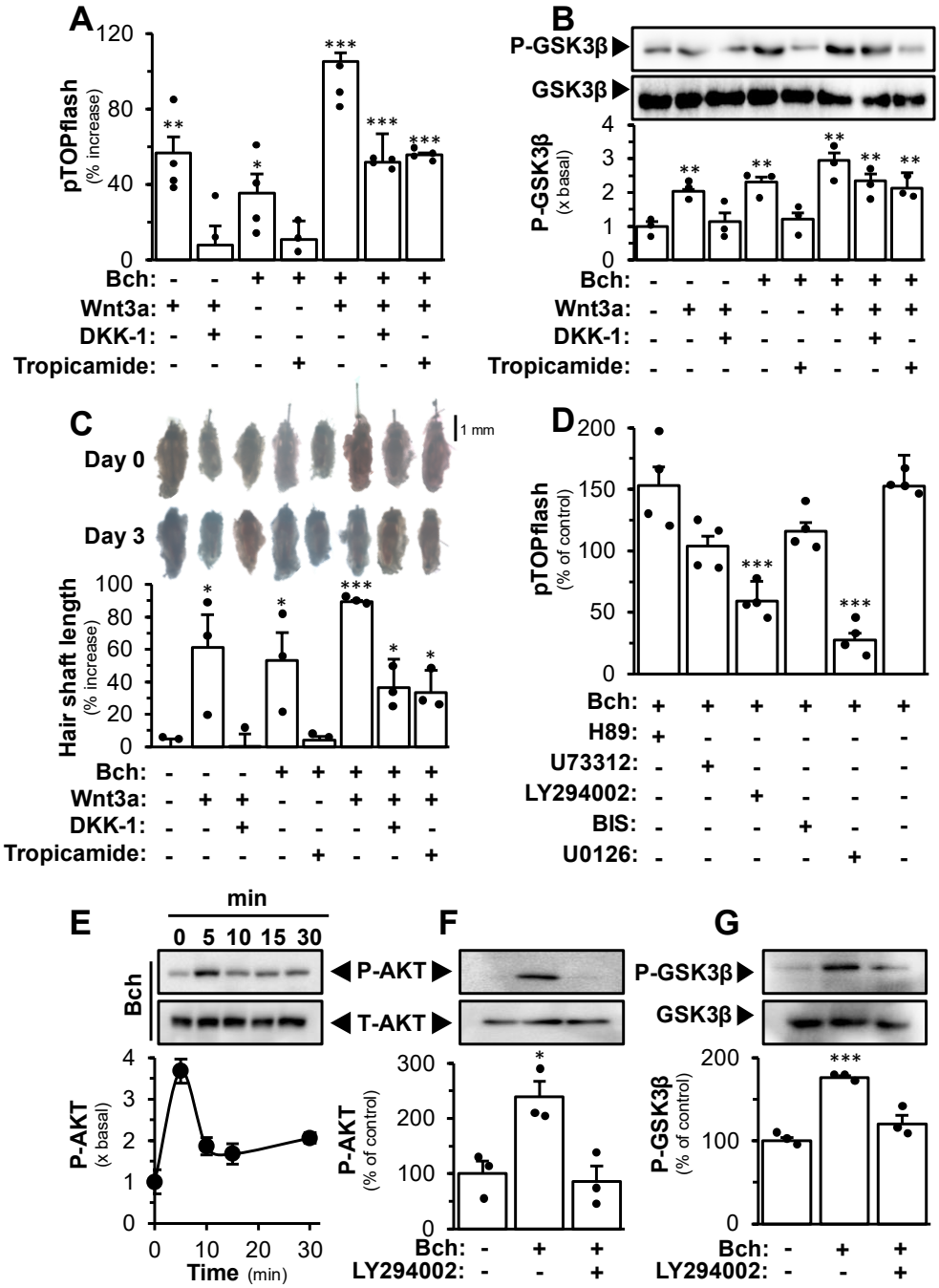

Figure 8. Mechanism of M4 mAChR in activating Wnt/β-catenin signalling. **(A):** The luciferase activity assay of pTOPflash-transfected DPC pre-treated with or without DKK-1 (300 ng/mL), or tropicamide (500 μM), for 30 min before the treatment of bethanechol (Bch; 5 mM), or Wnt 3a (200 ng/mL), or simultaneously with both treatments, for 24 hours. **(B):** Western blot of phosphorylated GSK3β (P-GSK3β) and total GSK3β from DPC which were subjected to the same treatment in (A). **(C):** The gross image of individual vibrissae subjected to the same treatment in (A) for 3 days were taken (upper). The measurement of hair shaft elongation was performed (lower). **(D):** The luciferase activity assay of pTOPflash-transfected DPC pre-treated or treated alone with H89 (10 μM), or U73312 (100 nM), or LY294002 (50 μM), or BIS (50 nM), or U0126 (10 μM) for 30 min before the treatment of bethanechol (5 mM) for 24 hours.

(E): Western blot of phosphorylated AKT (~60 kDa) and total AKT (~60 kDa) from DPC under bethanechol (5 mM) incubation for different times. **(F):** Western blot of phosphorylated AKT and total AKT as in (E) for 5 min, or preincubation with LY294002 (50 μM) for 30 min. **(G):** Western blot of phosphorylated GSK3β (P-GSK3β) and total GSK3β from DPC subjected to the same treatment in (F). Data are normalized and expressed as the % increase, % of control, or fold of basal value, in comparison to control, in mean ± SEM (n = 3-4), * $p < 0.05$, ** $p < 0.01$.

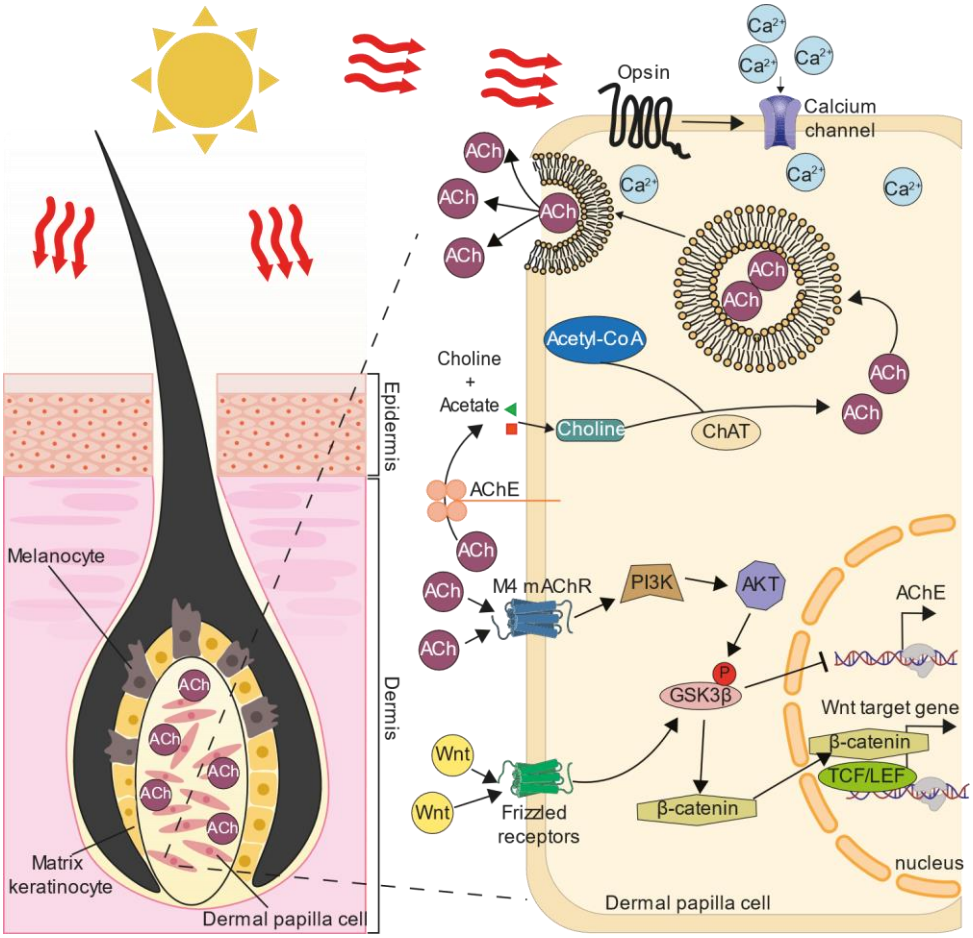

Figure 9. Proposed hypothesis for AChR in hair growth.

Under the stimulation of solar light, the influx of Ca^{2+} causes the release of ACh from DPC of hair follicle, and subsequently which acts as an autocrine agent in activating M4 mAChR. The activation of M4 mAChR can bypass the Frizzled and LRP5/6 receptors to activate the Wnt signalling by the phosphorylation of GSK-3β through the PI3K/AKT pathway. Together with the action of secreted Wnt proteins from hair follicle epithelium, the activation of Wnt/β-catenin signalling can be further augmented. The phosphorylated GSK-3β induced CREB DNA binding activity inhibit the expression of AChE, as a positive feedback loop.

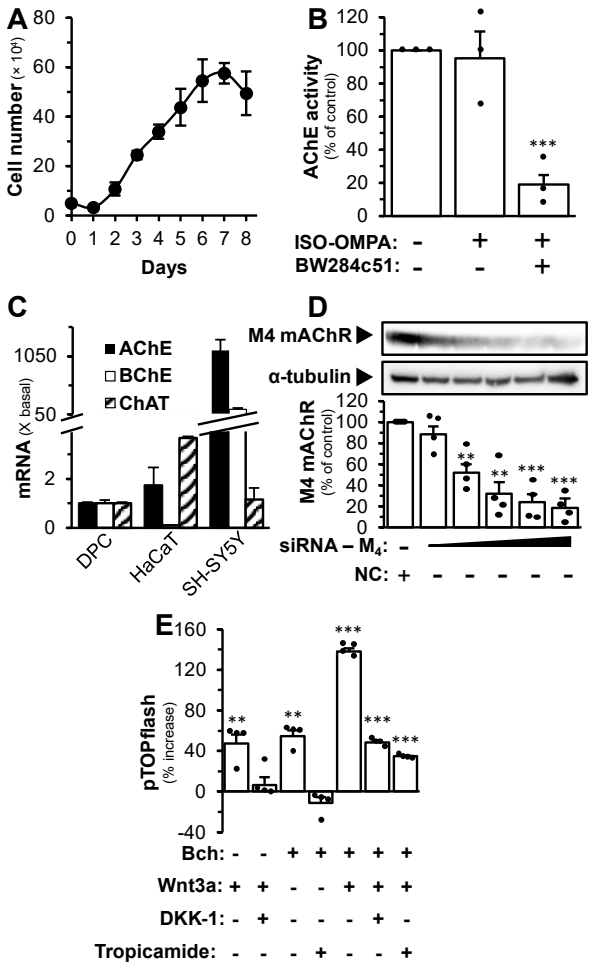

Supplementary Fig. 1. Cholinergic molecules in Wnt signaling.

(**A**): Growth curve analysis of DPC. (**B**): AChE activity of DPC treated with or without Iso-OMPA (50 μM) or BW284c51 (50 μM). (**C**): The mRNA levels of AChE, BChE and ChAT are shown in cultured DPC, HaCaT and SH-SY5Y. (**D**): Western blot of M4 mAChR (~55 kDa) and α-tubulin (~50 kDa) from DPC transiently transfected with siRNA-M_4 (0.625, 1.25, 2.5, 5, 10 nM, as indicated) or negative control (10 nM). (**E**): The luciferase activity assay of pTOPflash-transfected PC12 pre-treated with or without DKK-1 (300 ng/mL) or tropicamide (500 μM) for 30 min before the treatment of Bch (5 mM) or Wnt 3a (200 ng/mL) or simultaneously with both treatment for 24 hours. Data are normalized and expressed as the % increase, or % of control, or fold of basal (x basal), or in relative amount in comparison to control, in mean ± SEM (n = 4). ** $p < 0.01$.

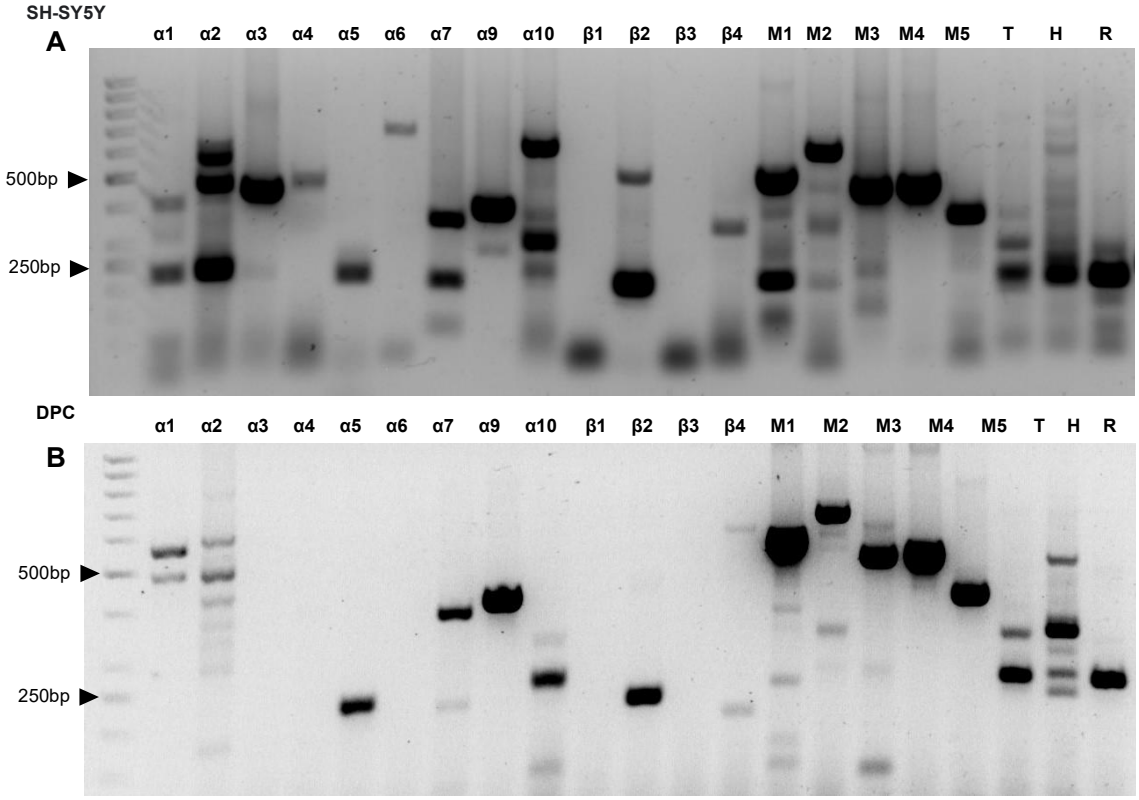

C

Gene	mRNA expression	Gene	mRNA expression
α1 nAChR	-	M1 mAChR	+
α2 nAChR	+	M2 mAChR	+
α3 nAChR	-	M3 mAChR	+
α4 nAChR	-	M4 mAChR	+
α5 nAChR	+	M5 mAChR	+
α6 nAChR	-	AChE	+
α7 nAChR	+	BChE	+
α9 nAChR	+	ChAT	+
α10 nAChR	+	CHT1	-
β1 nAChR	-	VAChT	+
β2 nAChR	+	OCT1	+
β3 nAChR	-	OCT2	-
β4 nAChR	-	OCT3	+

Supplementary Fig. 2. Subunits of AChR in DPC.

(**A**): DNA gel electrophoresis of PCR product of various subunits of nicotinic and muscarinic receptor of AChR in SH-SY5Y. (**B**): DNA gel electrophoresis of PCR product of various subunits of nicotinic and muscarinic receptor of AChR in DPC. (**C**): Summary of mRNAs of cholinergic molecules in DPC.

Primer	Sequence (5' to 3')	Primer	Sequence (5' to 3')
ALP (Forward)	AGC ACT CCC ACT TCA TCT GG	M1 mAChR (Reverse)	CGT GCT CGG TTC TCT GTC TC
ALP (Reverse)	TGT CTT CCG AGG AGG TCA AG	M2 mAChR (Forward)	CTC CTC TAA CAA TAG CCT GG
LEF-1 (Forward)	TTC CTT GGT GAA CGA GTC TG	M2 mAChR (Reverse)	GGC TCC TTC TTG TCC TTC TT
LEF-1 (Reverse)	GTG TTC TCT GGC CTT GTC GT	M3 mAChR (Forward)	GAC AGA AAA CTT TGT CCA CCC CAC
AXIN2 (Forward)	GGG AGA AAT GCG TGG ATA C	M3 mAChR (Reverse)	AGA AGT CTT AGC TGT GTC CAC GGC
AXIN2 (Reverse)	CTG CTT GGA GAC AAT GCT GT	M4 mAChR (Forward)	ATC GCT ATG AGA CGG TGG AA
IGF-1 (Forward)	TCA GAA GGG TAG CCC CTA GCT	M4 mAChR (Reverse)	GTT GGA CAG GAA CTG GAT GA
IGF-1 (Reverse)	TCA AGC CTG GGT ACT TTT AAC CA	M5 mAChR (Forward)	CTC ACC ACC TGT AGC AGC TAC CC
β-catenin (Forward)	CCC ACT AAT GTC CAG CGT TT	M5 mAChR (Reverse)	CTC TCT TTC GTT TGG TCA TTT GAT G
β-catenin (Reverse)	AAC CAA GCA TTT TCA CCA GG	AChE (All form; Forward)	AGA CCC CAA GGC CCC ACA AT
GAPDH (Forward)	ACC TGA CCT GCC GTC TAG AA	AChE-R (Reverse)	AGA GGG GTT ACA CCT GGC GG
GAPDH (Reverse)	TCC ACC ACC CTG TTG CTG TA	AChE-H (Reverse)	CAT GGG TGA AGC CTG GGC AG
α1 nAChR (Forward)	CGT CTG GTG GCAAAG CT	AChE-T (Reverse)	GGT GGA ACT CGG CCT TCC AC
α1 nAChR (Reverse)	CCG CTC TCC ATG AAG TT	AChE (Total; Forward)	GGG GCT CAG CAG TAC GTT AG
α2 nAChR (Forward)	GGA GCT CTG CCA CCC CCT AC	AChE (Total; Reverse)	CGG TGG CGC TGA GCA ATT T
α2 nAChR (Reverse)	AAC ATA CTT CCA GTC CTC	BChE (Total; Forward)	CTT TGT TGC AGA GAA TCG GAA ATC
α3 nAChR (Forward)	CTG GTG AAG GTG GAT GAA GT	BChE (Total; Reverse)	CGG TGG CGC TGA GCA ATT T
α3 nAChR (Reverse)	CTC GCA GCA GTT GTA CTT GA	ChAT (Forward)	AGC CCT GCC GTG ATC TTT G
α4 nAChR (Forward)	GGA TGA GAA GAA CCA GAT GA	ChAT (Reverse)	GCA CAG TCAGTG GGA ATG GAG T
α4 nAChR (Reverse)	CTC GTA CTT CCT GGT GTT GT	CHT1 (Forward)	TGC AGT ATC TCT GCC CTG TG
α5 nAChR (Forward)	TCA ACA CAT AAT GCC ATG GC	CHT1 (Reverse)	TGT GAT TCG CAT AAC CCA AA
α5 nAChR (Reverse)	CCT CAC GGA CAT CAT TTT CC	VAChT (Forward)	GTG CGC CAT GTC TCA GTC TA
α6 nAChR (Forward)	GTG GCC TCT GGA CAA GAC AA	VAChT (Reverse)	CAT AGA GCA GGT TGG CCA GT
α6 nAChR (Reverse)	AAT TATAAA TAC CCA AAG A	OCT1 (Forward)	GAC GCC GAG AAC CTT GGG
α7 nAChR (Forward)	CTT CAC CAT CAT CTG CAC CAT C	OCT1 (Reverse)	GGG TAG GCA AGT ATG AGG
α7 nAChR (Reverse)	GGT ACG GAT GTG CCAAGG ATAT	OCT2 (Forward)	CTA CAG TCC TCA TAA ATG CTG CAG C
α9 nAChR (Forward)	GTC CAG GGT CTT GTT TGT	OCT2 (Reverse)	GCT GAA GGG AGG CGG GTA GAG
α9 nAChR (Reverse)	ATC CGC TCT TGC TAT GAT	OCT3 (Forward)	GGA GTT TCG CTC TGT TCA GG
α10 nAChR (Forward)	CTC TCA AGC TGT TCC GTG ACC	OCT3 (Reverse)	GGA ATG TGG ACT GCC AAG TT
α10 nAChR (Reverse)	AAG GCT GCT ACA TCC ACG C	OPN1 (Forward)	TGT GCC TCT CTC CCT CAT CT
β1 nAChR (Forward)	CTA CGA CAG CTC GGA GGT CA	OPN1 (Reverse)	GGC ACG TAG CAG ACA CAG AA
β1 nAChR (Reverse)	GCA GGT TGA GAA CCA CGA CA	OPN2 (Forward)	GAG TCA GCC ACC ACA CAG AA
β2 nAChR (Forward)	ATG CCG TGG TCT CCT ATG AT	OPN2 (Reverse)	CAT GAA GAT GGG ACC GAA GTT GGA G
β2 nAChR (Reverse)	AGG GGA TGA TGA GGT TGA TG	OPN3 (Forward)	AGG AAC ACG AGG ATT CTT GC
β3 nAChR (Forward)	AGA GGC TCT TTC TGC AGA	OPN3 (Reverse)	GCG AGG GTC TGA GAG GAT AG
β3 nAChR (Reverse)	GCC ACA TCT TCA AAG CAG	OPN4 (Forward)	ACT CAG GAT GAA CCC TCC TTC
β4 nAChR (Forward)	GTG AAT GAG CGA GAG CAG AT	OPN4 (Reverse)	TGA ACA TGT TGG CAG GTG TC
β4 nAChR (Reverse)	GGG ATG ATG AGG TTG ATG GT	OPN5 (Forward)	CTA GAC GAA AGA AGA AGC TGA GAC C
M1 mAChR (Forward)	CAG GCA ACC TGC TGG TAC TC	OPN5 (Reverse)	GCG GTG ACA AAA GCA AGA GA

Supplementary Fig. 3. Sequences of primers for PCR.

The sequences of primers are listed. nAChR: nicotinic acetylcholine receptor. mAChR; muscarinic acetylcholine receptor. AChE-R: readthrough acetylcholinesterase. AChE-H: hydrophobic acetylcholinesterase. AChE-T: tailed acetylcholinesterase. CHT1: high-affinity choline transporter-1. OCT: organic cation transporters. OPN; opsin.